Actuator-line CFD simulation of tidal-stream turbines in a compact array

David D. Apsley

Abstract— **An actuator-line CFD model is used to simulate tidal-stream turbines acting alone or in a compact 3-turbine staggered array. CFD results confirm that the accelerated bypass flow between two proximal turbines in shallow water can enhance the power output for a close downstream turbine, with additional smaller effect of the upstream turbines' operating point. Comparison with other authors' experimental data in a narrow flume (IFREMER) and circular wave-current tank (FloWave) show some difference in relative loads between the turbines, possibly associated with ambiguity in overall blade pitch and difficulty in characterising onset flow in the FloWave tank. The accelerated bypass flow is persistent and largely established on the rotor plane of the upstream turbines, indicating how local array effects might be incorporated in simpler blade-element/momentum-theory design tools.**

Keywords—**tidal-stream turbines, CFD, actuator-line model, turbine array.**

I. Introduction

ALTHOUGH demonstration devices have been deployed at test sites such as the Bay of Fundy in Nova Scotia and the EMEC site in Orkney, and grid-connected turbines have been installed at the Meygen project in the Pentland Firth, tidal-stream energy represents a largely-unexploited renewable-energy resource. Its potential advantages include large energy density and predictable generation periods, without the infrastructure costs and environmental impact of tidal barrages. The high costs of installation, maintenance and grid-connection, however, have led to a focus on turbines which are large, of familiar and well-characterised types (3-bladed, horizontal-axis) and operate in arrays.

Whilst the general assumption in a wind-turbine array is that downstream turbines will suffer from the reduced momentum in the wakes of upstream devices, and therefore have to be far apart, the blockage effect associated with the free surface in shallow-water flow means that for tidal-stream turbines there will be an enhanced bypass flow outside the wakes of upstream devices and this may be exploited by laterally staggering a second row so as to experience an enhanced onset velocity. Indeed, since hydrodynamic power scales as the cube of the flow speed the potential benefits of this are huge.

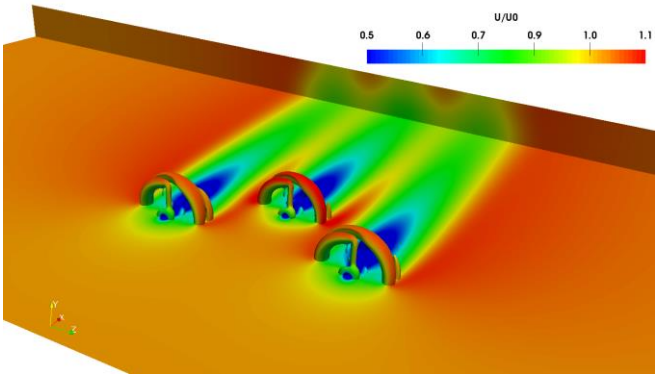

Fig. 1. CFD simulation of a compact 3-turbine array.

We would expect the largest benefits of this blockage-related enhancement to occur when the array is very compact and the water depth is small. One of the simplest arrays which can demonstrate this is a 3-turbine array arranged as in Fig. 1: two frontal turbines spaced such that their wakes just skirt a primary turbine situated in a staggered location a short distance downstream. The enhanced bypass flow can also be expected to be influenced by the flow deficit in the wake; i.e., by the operating point of the front turbines.

Reference [1] performed a series of experiments with such a three-turbine array at the University of Edinburgh's FloWave Ocean Energy Research facility. There they examined a multi-turbine array, with different combinations of operating speed of front and primary turbines. The objective of this research is to complement this with computer simulations. The array configurations are sketched in Fig. 2; this paper focuses on AC1 (single turbine) and AC3 (three-turbine array). In a three-turbine configuration the primary turbine, which is expected to experience the enhanced onset velocity, is $1D$ (one diameter) downstream of two front turbines whose hubs are $3D$ apart.

The main design tool for horizontal-axis wind and tidal turbines is blade-element momentum theory (BEMT). By

D.D. Apsley is a lecturer at the University of Manchester, Manchester M13 9PL, UK (e-mail: d.apsley@manchester.ac.uk).

Digital Object Identifier: https://doi.org/10.36688/ewtec-2023-195

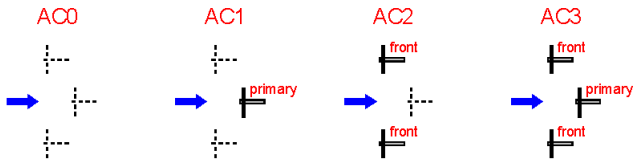

Fig. 2. Array configurations considered by [1].

equating axial force and turning moments on individual segments of blade from momentum theory with those from 2-d aerofoil theory, these loads may be determined and then integrated over the whole rotor to determine overall thrust, power and blade bending moment. Models can be improved by correcting for tip pressure leakage and high axial induction. A version of BEMT which is an improved version of that in [2] is used as a comparator in this paper. BEMT is extremely effective for individual turbines operating near their design point in a uniform onset flow. However, it is much less reliable when the flow is complex and ill-characterised, such as within an array. For the latter we turn to CFD.

In CFD simulations various representations of turbines are possible, ranging from simple actuator discs to fully-geometrically-resolved rotating devices. The former is too coarse for the time-dependent, complex flow within an array; the latter is too computationally expensive. A practical alternative, which permits the code to incorporate the principal geometric and hydrodynamic characteristics of turbine rotors, is an actuator-line model (ALM), which replaces the physical turbine by the reactive forces that it exerts on the flow. CFD-ALM has many advantages: it is much faster than a fully-resolved turbine model; there is no need for a complex rotating mesh; the background mesh is simple and can be decoupled from the individual turbines, making it straightforward to change individual rotor characteristics and the number or relative positions of devices in an array. Moreover, since it uses exactly the same turbine definitions as BEMT – radial distributions of blade twist and chord, and aerofoil lift and drag coefficients – it allows a consistent comparison with simpler models.

The structure of the rest of this paper is as follows. Section II describes the numerical solver and actuator-line model. Section III describes single-turbine characterisation in a flume at IFREMER facilities in France and in the University of Edinburgh's FloWave recirculating tank. Section IV examines the compact 3-turbine array studied at FloWave and compares CFD with experimental measurements as the operating points of both front and primary turbines are changed. Finally, Section V summarises the outcomes and discusses the direction of future research.

II. CFD Model

All CFD simulations in this paper were performed with an in-house CFD code STREAM. This is a RANS incompressible (or weakly-compressible) solver for multi-block structured grids. The code has the capability to solve for free-surface flows (e.g. waves) using a free-surface-following moving mesh and some preliminary simulations have been performed for turbines in waves. However, in the flows described here the Froude number is low and the upper surface is treated as a flat, stress-free rigid lid.

STREAM solves the standard conservative equations for continuity and momentum in time-dependent incompressible flow:

$$\frac{\partial U_j}{\partial x_j} = 0 \tag{1}$$

$$\frac{\partial(\rho U_i)}{\partial t} + \frac{\partial\left(\rho U_i U_j\right)}{\partial x_j} = -\frac{\partial P}{\partial x_i} + \frac{\partial}{\partial x_j}\left(\mu\frac{\partial U_i}{\partial x_j} - \rho\overline{u_i' u_j'}\right) \tag{2}$$

Here, t is time, x_i are space coordinates, ρ is density, μ is dynamic viscosity, P is pressure, U_i and u_i' are mean and turbulent velocity components respectively. A large number of RANS turbulence models for the Reynolds stress $-\rho\overline{u_i' u_j'}$ are available in STREAM, but only simple eddy-viscosity models of $k-\varepsilon$ and $k-\omega$ type have been deployed in this study; this leads to two extra transport equations for the turbulence variables. Advective fluxes are discretised using the third-order UMIST scheme and temporal derivatives by the second-order Crank-Nicolson scheme. Variable storage is co-located and cell-centred, necessitating use of Rhie-Chow interpolation for advective fluxes. The heavily coupled equations for mean and turbulent variables are solved iteratively at each timestep using the SIMPLE pressure-correction method.

The ALM employed in the code is described in [2],[3], so only a short summary will be given here. Reference [2] considered a wind turbine on a floating platform (in the device frame, equivalent to a time-varying onset flow). Reference [3] addressed a multi-turbine tidal-stream array (but much less compact than that addressed here), with rotor speed allowed to change in response to hydrodynamic load.In the present simulation and experiments the turbines are speed-controlled and there is assumed to be a time-steady and uniform onset flow.

In an ALM there is no solid surface to displace the flow, but the physical turbine blades are replaced by the reactive force distribution that they exert on the fluid. In discrete form the fluid force on a short blade segment of radial length Δr and local chord c is

$$\mathbf{F}_p = \frac{1}{2}\rho U_{\mathrm{rel}}^2 (c\Delta r)(C_D\hat{\mathbf{e}}_D + C_L\hat{\mathbf{e}}_L) \tag{3}$$

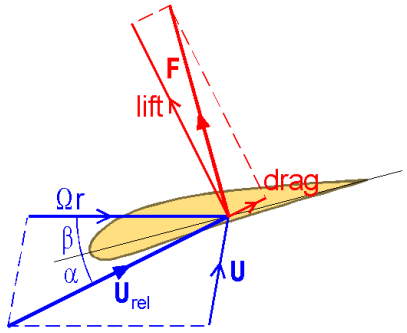

Fig. 3. Definition of angles and velocity and force components for a single blade segment.

where $C_D(r,\alpha)$ and $C_L(r,\alpha)$ are aerofoil drag and lift coefficients determined from pre-computed look-up tables, $\mathbf{U}_{\rm rel}$ is the flow velocity relative to the blade, formed by the vector sum of interpolated velocity at the actuator point (minus any radial component) and the $-\Omega r$ relative velocity due to rotation, α is the angle of attack (determined – see Fig. 3 – from $\mathbf{U}_{\rm rel}$ and the local blade twist β) and $\hat{\mathbf{e}}_D$ and $\hat{\mathbf{e}}_L$ are unit vectors in the drag and lift directions, respectively. As point sources would give a very "spiky" force distribution, a continuous body-force density is created by distributing the reactive force over a finite region, typically by a gaussian distribution:

$$\mathbf{f}(\mathbf{x}) = -\mathbf{F}_p \frac{\mathrm{e}^{-(\mathbf{x}-\mathbf{x}_p)^2/\sigma^2}}{\sigma^3\pi^{3/2}} \tag{4}$$

where $\mathbf{x}_p$ and $\mathbf{x}$ are actuator and field points respectively. The spread parameter σ varies [2] as

$$\sigma = \max\left(\sigma_m\sqrt{1-(2r/R-1)^2}, 2\Delta_g\right) \tag{5}$$

where $\sigma_m = 0.038D$, D is the rotor diameter and $\Delta_g = (\text{volume})^{1/3}$ is the local grid size. Unlike BEMT, no explicit tip correction is necessary for actuator-line CFD, since any leakage flow from pressure to suction surfaces should be resolvable. In this study the background mesh is Cartesian, so that, since the exponential function factorises coordinatewise, the integrals of body force over control volumes can be evaluated directly in terms of products involving the error function erf(x):

$$\int_{x_1}^{x_2} \exp\left[-\left(\frac{x-x_p}{\sigma}\right)^2\right] \mathrm{d}x = \sigma\frac{\sqrt{\pi}}{2}\left[\mathrm{erf}\left(\frac{x_2-x_p}{\sigma}\right) - \mathrm{erf}\left(\frac{x_1-x_p}{\sigma}\right)\right] \tag{6}$$

This avoids the numerical quadrature required for non-Cartesian grids, ensures that the integrated force is correct and is efficiently evaluated by a standard library function in Fortran.

III. Single-Rotor Comparison

Before array comparisons, baseline simulations for a single turbine of identical design have been undertaken. Experimental results are available from narrow-flume testing at the IFREMER facilities in Boulogne-Sur-Mer [4] and wide-tank tests performed as part of the array tests at FloWave in Edinburgh [1].

1) *Comparison with data from the IFREMER flume.*

The rotor used in this study was developed for a larger EPSRC-funded project (X-MED). Its design and manufacture are described in detail in [4], accompanied by measurements of thrust and power measurements and a small number of wake velocity measurements in a flume at IFREMER's flow facilities. The simulations reported in the current paper are compared with the electronic dataset linked to the online version of that reference.

The turbine rotor is three-bladed, with rotor and nacelle diameters of 1.2 m and 0.12 m, respectively. Blades are generated from NACA 63-8xx aerofoil sections. Radial variations of twist, chord and aerofoil thickness are tabulated in [4], whilst drag and lift coefficients for a representative set of sections have been precomputed using XFoil [5]. Additional global pitch can be adjusted at blade root via a mounting plate; the simulations here suggest considerable sensitivity to that parameter.

The turbine was tested at mid-depth in a flume with cross-stream dimensions 4 m wide × 2 m deep. This gives a high blockage ratio of 14%, yielding thrust and torque that are significantly higher than in unbounded flow. Experiments and CFD-ALM simulations were compared directly with the prescribed cross-section blockage. However, in order to compare with BEMT, an analysis was also conducted with a blockage correction [6] to "open-water" conditions.

For the CFD-ALM calculations a 115 (streamwise) × 90 (depthwise) × 110 (spanwise) cell mesh was used, extending 3D upstream and 7D downstream of the rotor. Both sides and the top and bottom boundaries were treated as symmetry planes, and uniform conditions were prescribed for transported variables at inlet. In the flume the onset flow velocity is 0.81 m s^{-1}, giving a Reynolds number based on onset velocity and rotor diameter of 9.7×10^5. Onset turbulence levels of 3% and 12% were investigated, but both experiments and CFD simulations suggest that the mean thrust and power were insensitive to these. The present simulations used an onset turbulence intensity of 3%. In the absence of production from velocity shear, an artificially high turbulent lengthscale (or low dissipation rate) has to be prescribed at inlet in order to maintain the specified turbulent intensity as far as the rotor. From impulsive start, steady loads were obtained after one domain pass-through time, requiring about 6

hours on 8 processors of the University of Manchester's Computational Shared Facility (CSF).

In this paper quantitative load data is presented in terms of thrust, power and (flapwise) root bending-moment coefficients, defined as

$$C_T = \frac{\text{thrust}}{\frac{1}{2}\rho U_0^2 A}, \quad C_P = \frac{\text{power}}{\frac{1}{2}\rho U_0^3 A}, \quad C_{FBM} = \frac{\text{flapwise bending moment}}{\frac{1}{2}\rho U_0^2 A R} \tag{7}$$

where $D = 2R$ is the diameter of the rotor, $A = \pi D^2/4$ is the swept area and U_0 is the onset velocity. The tip-speed ratio is

$$\text{TSR} = \frac{\Omega R}{U_0} \tag{8}$$

where Ω is the angular velocity of the rotor. Thrust and flapwise bending moment depend on axial force components, whilst power (= torque × angular velocity) depends on azimuthal force components.

It was observed early on for the simulations of both IFREMER flume (blockage-corrected) and FloWave tank that the values of thrust determined experimentally were somewhat less than those produced by BEMT and CFD-ALM approaches and, indeed, with many similar turbines. A possible explanation is the considerable sensitivity of aerofoil lift (and, hence, thrust and bending moment) to blade pitch and consequent angle of attack. It is unclear how accurately pitch was set using the angular-adjustment mechanism. Accordingly, an investigation of sensitivity to blade pitch was carried out with BEMT. Results are shown in Fig. 4. CFD-ALM simulations, which are based on the same aerofoil parameters, would be expected to show similar sensitivity. Consistent with changes to aerofoil lift, but not drag, thrust coefficient at typical TSR (say, 6) decreases by about 12% as hub pitch varies from 0° to 2°, whereas power coefficient does not change significantly over this range. As both BEMT and ALM simulations support substantially better agreement with experimental results with an additional hub pitch of 1°, a pragmatic decision was taken to use this for calculations in the remainder of this paper.

Fig. 5 shows (uncorrected) thrust and power coefficients measured in the IFREMER flume and CFD-ALM calculations with two common RANS turbulence models: $k-\omega$ SST [7] and standard $k-\varepsilon$ model [8]. Note that, in contrast to a fully-resolved physical turbine blade, the ALM model introduces no solid boundaries, so the distinct boundary-layer behaviour of these turbulence models is not tested. Although at this level of turbine representation there is very little to choose between the two models, there is marginally better agreement with the $k-\omega$ SST model, so this has been used for the remainder of the simulations.

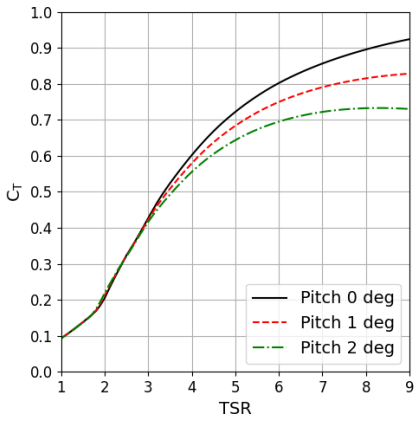

(a)

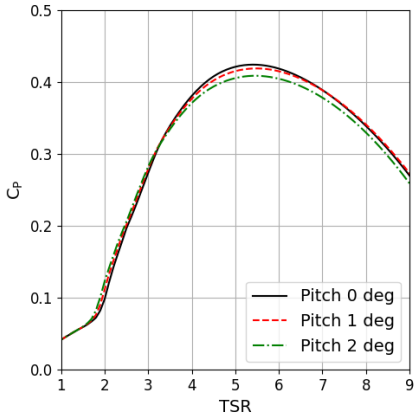

(b)

Fig. 4. BEMT predictions of (a) thrust and (b) power coefficients as a function of TSR with different blade pitch.

As the turbine in the IFREMER flume has a very high blockage ratio, more representative loads can also be presented by using a blockage correction (Fig. 6). This reduces both C_T and C_P by about 0.05, or some 10% in the case of the power coefficient. In this unblocked scenario we can also compare results with the much faster BEMT approach. Over the limited range of TSR covered in the experiments (note that the power curve, in particular, is very flat) all methods give similar results for turbine loads.

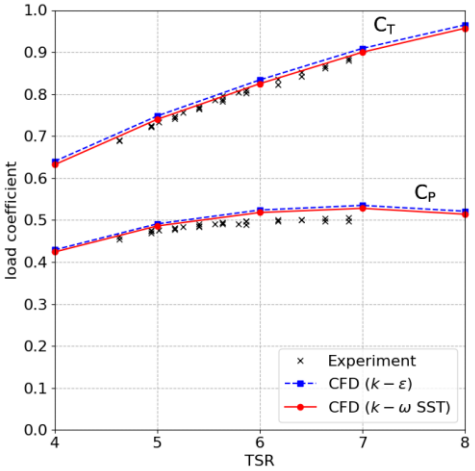

Fig. 5. Thrust and power coefficients in the IFREMER flume; actual flume dimensions and no blockage correction.

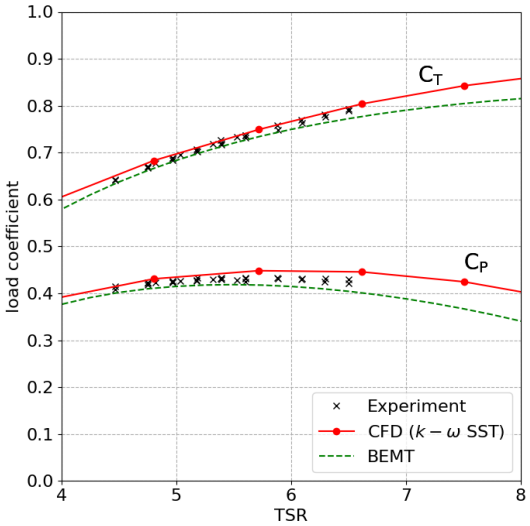

Fig. 6. Thrust and power coefficients in the IFREMER flume; with blockage correction.

BEMT loads tend to be lower than their CFD counterparts at the high and low ends of the TSR range, but there is no experimental data to compare with here.

Fig. 7 shows the streamwise mean velocity simulated on the turbine centreline. The figure suggests that the impact of the turbine begins to be felt $1.5-2D$ upstream of the rotor. There is a surprising insensitivity of the wake velocity deficit to operating point, with velocity recovering to about 80% of the onset velocity some $4D$ downstream of the rotor plane irrespective of TSR, despite the thrust on the rotor (and hence the overall momentum extracted from the flow) increasing by about 40% over this range. The differences due to turbulence model are more significant than those due to rotational speed, but are still small.

2) Comparison with data from the FloWave tank.

Reference [1] performed experiments with 1 to 3 turbines identical to those in Section III(1) within the University of Edinburgh's FloWave Ocean Energy Research Facility. This is not a rectangular flume but a circular facility of diameter 25 m designed to accommodate simultaneous waves and currents. A set of impellers drives a flow which is reasonably uniform (±10%) through a central region of plan area 50 m², with nominal velocity 0.8 m s⁻¹ over a depth of 2 m. This subsection describes the single-turbine simulations (AC1); Section IV will address the 3-turbine arrays (AC3).

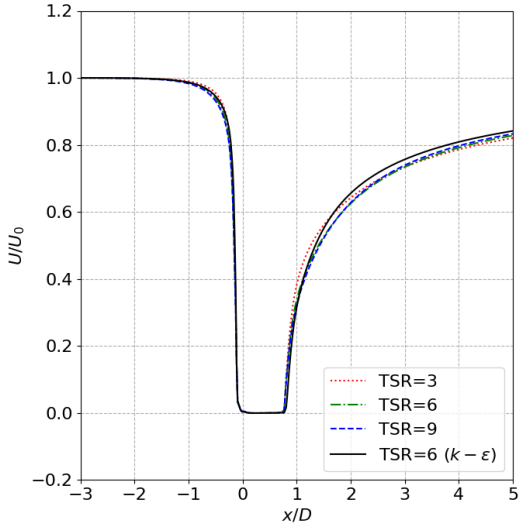

Fig. 7. Velocity on the centreline in the IFREMER flume.

It is not practical to simulate the circular tank geometry, which includes recirculating pumps, multiple individually-controlled inlets and flow conditioners. For the present work a cuboid domain of spanwise width equal to the diameter of the tank (25 m, or $20.8D$), and depth 2 m ($1.67D$), was adopted. The global blockage ratio per turbine (2.3%) was deemed insignificant. For consistency, and to permit a direct comparison between 1-turbine and 3-turbine simulations, the same computational domain and mesh was used for each. A 16-block computational domain extends $4D$ upstream of the primary turbine ($3D$ upstream of the front turbines where installed) and $5D$ downstream of the primary turbine. The mesh (Fig. 8) consists of just over 1.8 million cells, with resolution $0.02D$ across all 3 turbine rotors (even when the front rotors are not installed). Very little grid resolution is required at the spanwise sides, the function of cells here being simply to enforce the desired blockage. Accordingly, the two outer blocks are comprised of large cells interfaced non-conformally to the central blocks.

The electronic database tied to the online version of [1] contains (absolute) thrust, power and flapwise bending moment, together with a small amount of velocity data, mainly on turbine centrelines. To recover non-dimensional coefficients an overall onset velocity is required. For the single-turbine simulations, which are slightly less sensitive to spatial and device-dependent inhomogeneity in the FloWave tank, the measured velocity at $2D$ upstream of the rotor was used ($U_0 = 0.775$ m s^{-1}). Inflow turbulence intensity was set at 8% to match measurements. An unphysically large length scale (or small dissipation) was set at inflow to minimise losses of turbulence energy upstream of the rotors. Other boundary conditions were the same as Section III(1). No blockage corrections were applied here.

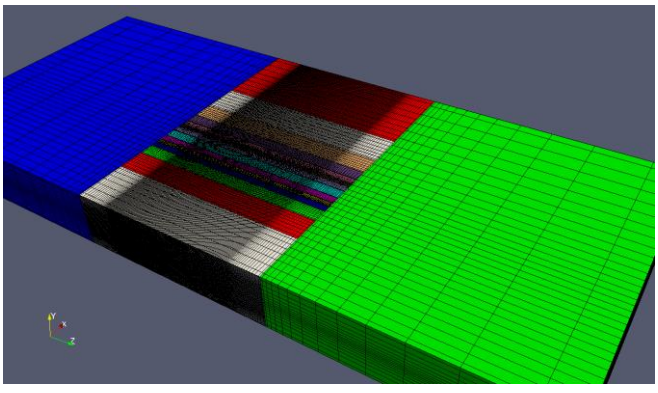

Fig. 8. Computational mesh for the FloWave simulations.

Fig. 9 shows a comparison of computed and measured thrust, power and flapwise bending-moment coefficients as a function of TSR. Since thrust and blade bending moments vary as velocity squared, whilst power varies as velocity cubed, the magnitude of these coefficients is very sensitive to the difficult-to-specify onset velocity. As noted earlier, CFD simulations with the nominally-unpitched blades gave thrust (but not power) magnitudes substantially higher than experiment. Better agreement is obtained with an additional 1° pitch, but the comparison is nowhere near as satisfactory as for the flume results in Section III(1), despite this being nominally an identical turbine. Thrust coefficients C_T based on the experimental measurements also appear to be on the low side for typical turbines. Possible explanations include the difficulty in prescribing onset flow velocity U_0 and the non-uniformity of the flow (in the vertical and the horizontal) in the measurement area of the circular tank.

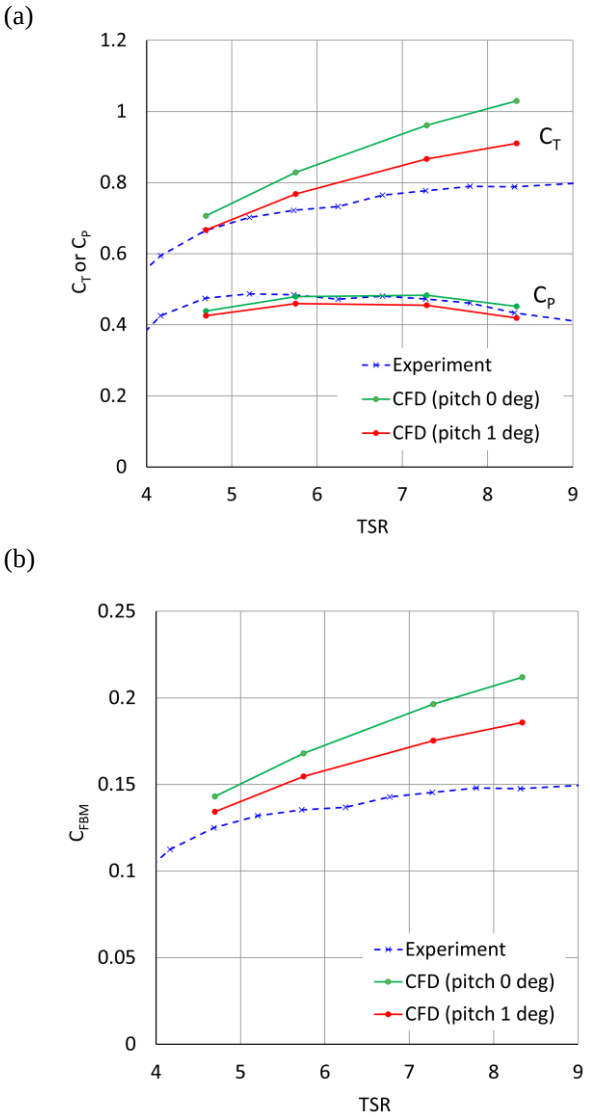

Fig. 9. Load coefficients for the single-turbine case (AC1): (a) thrust and power; (b) flapwise bending moment.

IV. THREE-TURBINE SIMULATIONS

This section describes the three-turbine (AC3) configuration of Fig. 2, which was investigated experimentally in [1]. Here the "primary" turbine is $1D$ downstream of, and staggered symmetrically from, two "front" turbines, whose centres are $3D$ apart. All turbines rotate in the same sense, with individually-controlled speeds. In the overview (Fig. 1) one can observe the predicted magnitude of velocity on the array centreplane and in the tip vortices (identified by isosurfaces of the Q vorticity parameter). On the central plane an enhanced bypass flow impinges on the downstream rotor and is expected to deliver an enhanced power output. In Fig. 1 all rotors rotate at 90 rpm (TSR ≈ 7.1), but when operating at different rotational speeds the greater thrust on the front turbines should lead to greater velocity deficit in the wake and, in consequence, greater bypass flow. Thus, this research also examines the response of the primary turbine to changes in the operating point of the front turbines.

The CFD simulations of this Section use the same mesh and the same (non-dimensional) boundary conditions as Section III(2). For direct comparison of load coefficients with the experimental data (where loads were only specified in absolute N and m units) an absolute value of onset velocity is required. Here, the observed variation with installed devices and non-uniformity of flow within the FloWave tank presents some challenges. As in Section III(2) it has been decided to use the velocity on the array centreline a distance $2D$ upstream of the primary turbine. With three turbines installed this is $U_0 = 0.756\ \mathrm{m\ s^{-1}}$, slightly smaller than the single-turbine case.

Figure 10 shows the CFD-simulated centreline mean velocity for the primary turbine, comparing an isolated turbine (dashed line) against a 3-turbine array (solid line) for the cases where all turbines rotate at 90 rpm (nominal TSR about 7.1). With an isolated single turbine the streamwise velocity responds to the presence of the device from about 2D upstream of the rotor disk, and falls monotonically as it approaches the turbine. However, with the 3-turbine array the velocity field is boosted by the local blockage effect between the front turbines, and there is an initial *increase* in velocity on the plane of the upstream rotors, 1D upstream of the primary rotor. Downstream of the primary turbine the centreline velocity field ostensibly appears to recover more rapidly, but this is an artefact of the actual onset flow to this turbine being faster.

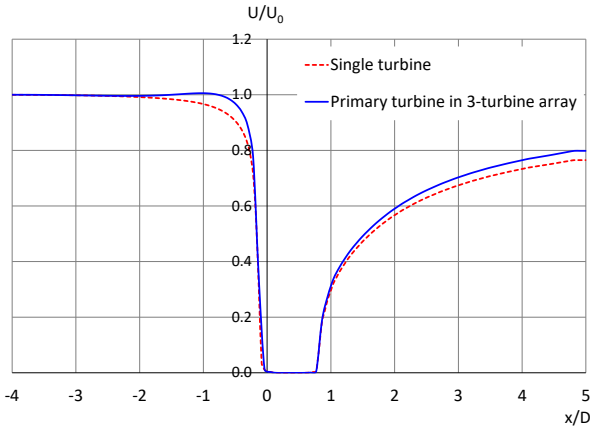

Fig. 10. Mean-velocity profile on the primary-turbine centreline.

Fig. 11 is the most important figure of this paper. It demonstrates how loads – thrust, power and bending moment – on the primary turbine increase as a result of the enhanced onset flow induced by staggered turbines a short distance usptream. In this figure the primary (downstream) turbine operates at 90 rpm (other speeds demonstrate similar results) and the graphs show the load characteristics when there are are either no front turbines (case AC1) or front turbines operating at speeds 58, 71, and 90 rpm. Note that a single velocity scale – the array onset velocity, U_0 – is used to normalise C_T, C_P and C_{FBM}, irrespective of the actual onset velocity to each turbine.

As already noted for an isolated turbine in the FloWave tank (but not in the IFREMER flume) there are differences in the absolute size of each load coefficient between experiment (dashed lines) and computation (solid lines). This is more significant for axial force components (contributing to thrust and bending moment) than azimuthal forces (contributing to power), suggesting a dependence on lift associated with blade pitch. Nevertheless, despite this difference in baseline, experiments and computations clearly demonstrate similar key features. (1) The mere presence of closely-spaced upstream turbines raises loads significantly on the primary turbine, because of the locally-increased bypass velocity induced by the blockage effect. (2) Increasing the speed of the front turbines augments loads, because of more momentum loss in the front-turbine wakes and consequent enhancement to the bypass flow. (3) The speed effect is, however, much smaller than that arising from physical presence alone, indicating that the positioning of turbines is more important than their operating point. (4) The greatest relative uplift in loads is for power rather than thrust or bending moment, since power typically scales on velocity cubed rather than velocity squared. At (array-based) TSR = 7 the increases in thrust, power and bending moments are predicted to be 11%, 21% and 10% respectively. These correspond to an effective onset velocity increase in the range 3–6% (if changes to position on the turbine characteristics are neglected).

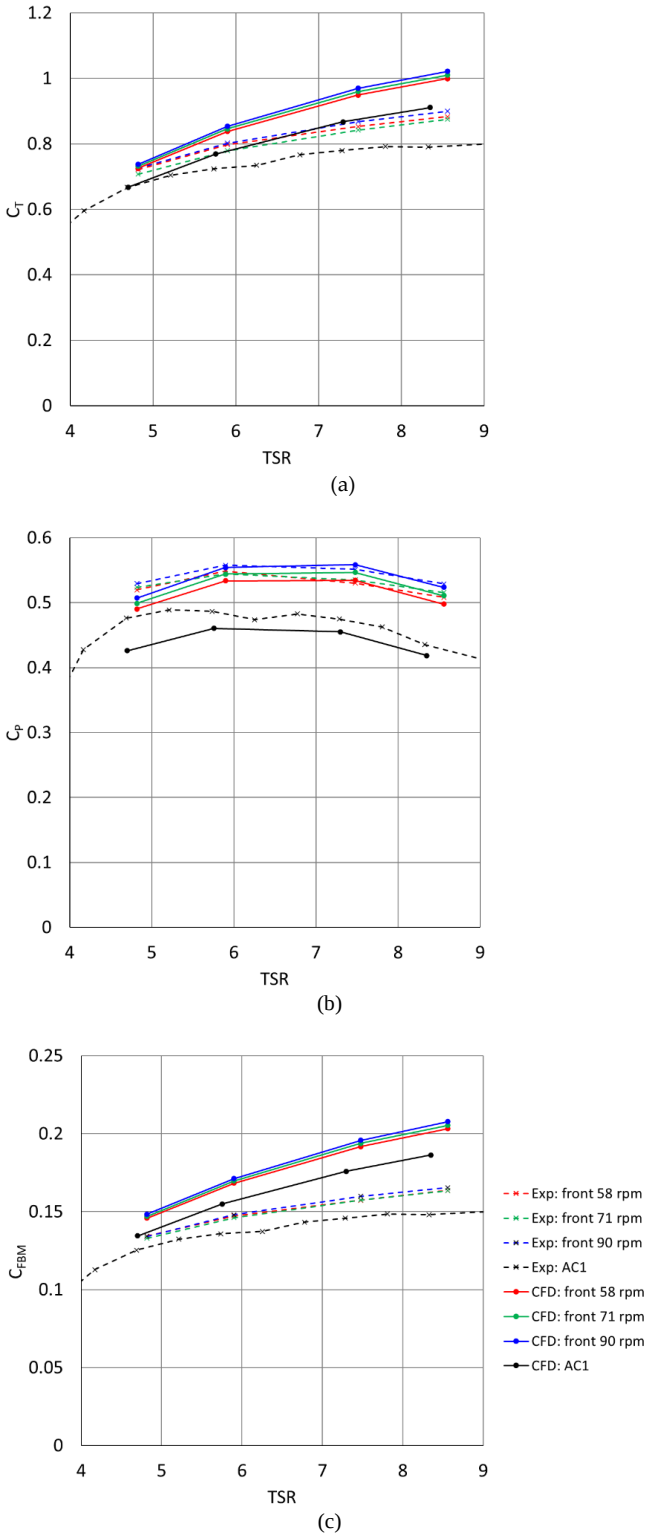

Fig. 11. Three-turbine array; load coefficients of the primary turbine for different rotation rates of the front turbines: (a) thrust; (b) power; (c) flapwise bending moment..

Fig. 12 shows lateral profiles of streamwise mean velocity in the wake of single (AC1; dashed lines) and multiple (AC3; solid lines) turbine arrays. In both cases there is still a clear signature of the turbines at the furthest extent of the computational domain ($x/D = 5$). Due to enhanced local blockage, the bypass flow velocity is larger for the 3-turbine case. Overall, this bypass speedup is quite

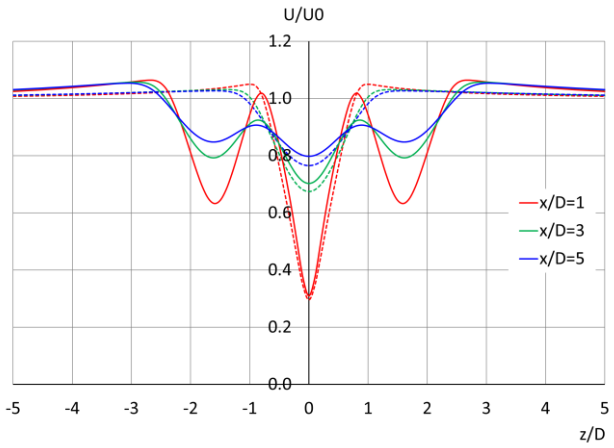

Fig. 12. Cross-stream mean-velocity profile at various distances downstream of the primary turbine; solid lines – three-turbine array; dashed lines of the same colour – isolated turbine.

large, is detectable laterally for several diameters, and, importantly from the perspective of designing simple array models, evolves slowly in the streamwise direction, being essentially established on a rotor plane.

However, although the load changes on the *primary* turbine due to the presence and operating point of upstream staggered turbines is, at least qualitatively, similarly predicted by CFD and experiment, there is a disappointing disagreement when it comes to the *front* turbines, which were – nominally at least – identical to the primary turbine. Unfortunately, the investigators in [1] chose not to plot or discuss these in their paper; the data for comparison here is drawn solely from the tied electronic database.

Many different speed combinations have been computed, but Figure 13 shows representative cases, with the primary turbine operating at 90 rpm (TSR a little over 7) and two front turbine speeds. Thrust and power coefficient, normalised by array velocity, are plotted in left and right columns.

Here, and for other speed combinations, CFD results turn out to be very much in line with expectations. (1) The loads on each of the front turbines are exactly the same as for an isolated turbine (i.e. at these separations they are not affected by the presence of spanwise and downstream neighbours). (2) At the same rotational speed, loads on the downstream primary turbine are higher than those on the front turbines because of the accelerated bypass flow. By contrast, however, the experimental database records loads on the front turbines which are significantly higher than single turbines in isolation and, in the 90/90-rpm case, higher than the loads on the primary turbine. If the turbines are truly identical and subject to a uniform onset flow then this is implausible. Possible explanations include that the turbines have not been set up identically (for example, with global blade pitch), or that force sensors have been differently calibrated. However, the most likely explanation is the variation of velocity in the measurement region of the FloWave tank. [1] cites a variation of ±10% in velocity, which translates to a potential variations in thrust of order ±21% and of power ±33%: certainly more than enough to cause the deviations here. Additionally, it makes the task of identifying a true array-onset velocity for normalising load coefficients quite difficult.

V. CONCLUSIONS

CFD with an actuator-line representation of turbine blades has been used to simulate loading on model tidal-stream turbines, as individual devices or in an array of 3 turbines. In contrast to previous small-array studies, the array configuration is very compact, with emphasis on the

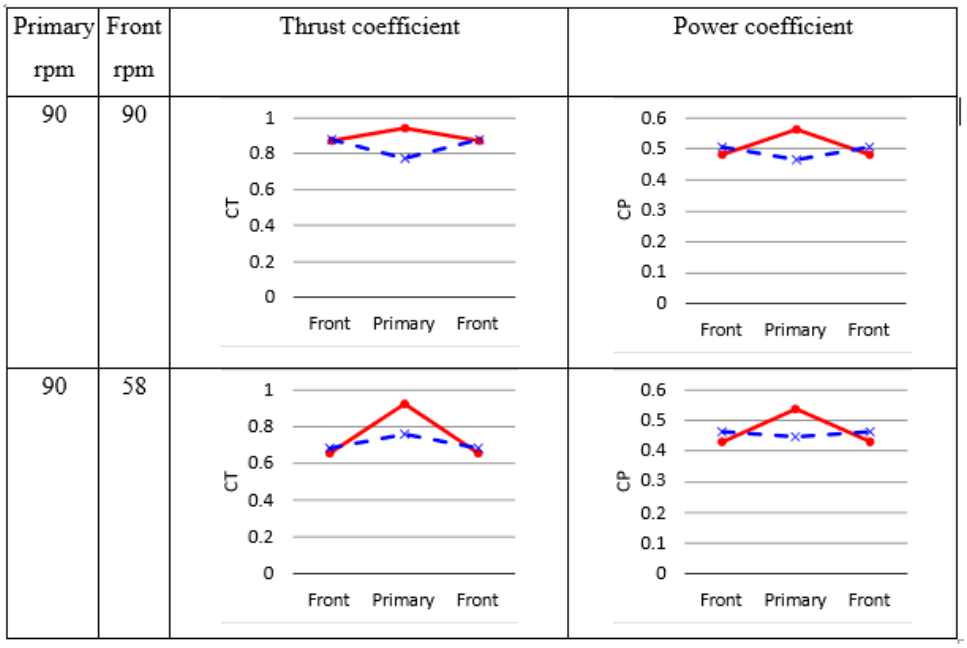

Fig. 13. Thrust coefficient, C_T, and power coefficient, C_P, for various rotation speeds in a three-turbine array; dashed blue lines are experimental data; solid red lines are CFD. (All turbine coefficients have been normalised using the same array onset velocity.)

possibility of siting two proximal turbines in such a way as to enhance the onset flow to a third turbine. Comparison has been made with experiments (and, for isolated turbines, with BEMT) in a narrow flume (IFREMER) and in a shallow circular tank (Edinburgh FloWave).

BEMT and CFD-ALM show a considerable sensitivity of axial loads (thrust and flapwise bending moment), but not azimuthal loads (torque, and hence power) to blade pitch. To obtain reasonable agreement with experiment it has been found necessary to make a 1° adjustment to the nominal published blade twist. This then yielded excellent agreement with the IFREMER flume data, but still a modest over-prediction of axial load coefficients for the FloWave dataset. An additional difficulty for the second dataset was to identify an appropriate onset velocity, due to flow non-uniformity in the tank.

Both CFD simulations and experimental measurements demonstrate the possibility of exploiting blockage effects within a dense, but staggered, arrangement of turbines, together with proximal bed and free surface, to increase the onset flow to downstream turbines, thereby increasing hydrodynamic power. Simulations and experiments also reveal an additional (but smaller) augmentation dependent on the upstream turbines' operating point.

Velocity fields extracted from the CFD simulations reveal an enhancement to the bypass flow resulting from limited-depth effects that is set up on the rotor plane and evolves comparatively slowly with distance downstream. This is a useful observation in that it would allow relatively cheap array-superposition models based on the semi-anaytical and much faster BEMT approach to be satisfactorily adapted for turbine arrays.

Although the behaviour of the primary turbine in proximity to two turbines upstream is, at least qualitatively, well simulated, there is disagreement with the loads on the front turbines. At $3D$ between centres CFD (as expected) predicts these to behave like isolated turbines, whereas experimental data (available in the database, but not commented on in the associated journal paper [1]) suggests that loads on these are significantly higher. This difficult-to-explain observation is most likely to be due to the documented non-uniformity of velocity in the circular FloWave tank.

REFERENCES

[1] D.R. Noble, S. Draycott, A. Nambiar, B.G. Sellar, J. Steynor and A. Kiprakis, "Experimental assessment of flow, performance and loads for tidal turbines in a closely-spaced array", *Energies*, vol. 13, no. 1977, 2020. [Online].

[2] D.D. Apsley and P.K. Stansby, "Unsteady thrust on an oscillating wind turbine: Comparison of blade-element momentum theory with actuator-line CFD", *Journal of Fluids and Structures*, vol. 98, 2020. [Online].

[3] D.D. Apsley, T. Stallard and P.K. Stansby, 2018, "Actuator-line CFD modelling of tidal-stream turbines in arrays", *Journal of Ocean Engineering and Marine Energy*, vol. 4, pp. 259-271, 2018.

[4] G.S. Payne, T. Stallard and R. Martinez, "Design and manufacture of a bed supported tidal turbine model for blade and shaft load measurement in turbulent flow and waves", *Renewable Energy*, vol. 107, pp. 312-326, 2017.

[5] M. Drela, "XFOIL: An analysis and design system for low Reynolds number airfoils", *Low Reynolds Number Aerodynamics. Lecture Notes in Engineering*, T.J. Mueller. (ed), vol. 54, Springer, Berlin, Heidelberg, 1989.

[6] A.S. Bahaj, A.F. Molland, J.R. Chaplin and W.M.J. Batten, "Power and thrust measurements of marine current turbines under various hydrodynamic flow conditions in a cavitation tunnel and a towing tank", *Renewable Energy*, vol. 32, pp. 407–426, 2007.

[7] F.R. Menter, "Two-equation eddy-viscosity turbulence models for engineering applications", *AIAA J.*, vol. 32, pp. 1598-1605, 1994.

[8] B.E. Launder and D.B. Spalding, "The numerical computation of turbulent flows", *Computer Meth. Appl. Mech. Eng.*, vol. 3, pp. 269-289, 1974.